Journal of Alloys and Compounds 797 (2019) 702–709

Contents lists available at ScienceDirect

Journal of Alloys and Compounds

journal homepage: http://www.elsevier.com/locate/jalcom

Ultrathin NiO confined within hollow carbon sphere for efficient electrochemical energy storage

Xiaoze Shi [a], Shuai Zhang [a], Xuecheng Chen [a, b, *], Tao Tang [b, **], Rüdiger Klingeler [c], Ewa Mijowska [a, ***]

[a] Nanomaterials Physicochemistry Department, Faculty of Chemical Technology and Engineering, West Pomeranian University of Technology, Szczecin, Piastów Ave. 42, 71-065, Szczecin, Poland
[b] State Key Laboratory of Polymer Physics and Chemistry, Changchun Institute of Applied Chemistry, Chinese Academy of Sciences, Changchun, 130022, China
[c] Kirchhoff-Institut für Physik, Universität Heidelberg, INF 227, D-69120 Heidelberg, Germany

ARTICLE INFO

Article history:
Received 8 March 2019
Received in revised form
9 May 2019
Accepted 13 May 2019
Available online 15 May 2019

Keywords:
NiO
Hollow carbon spheres
Lithium-ion batteries
Supercapacitor

ABSTRACT

In this contribution, we present a facile encapsulating process for controlled synthesis of a hybrid structure of ultrathin NiO crystals confined growth on the interior shells of hollow carbon sphere (NiO@HCS). In this method, a complete HCS with high porosity and good electrical conductivity can selectively confine the growth of NiO directly to its inner carbon shell. The as-prepared NiO@HCS offers advantages such as high surface area, great electrical conductivity and suitable pore size distribution. Besides, the small number of metal oxide nanocrystals inside HCS can provide more efficient electrochemical reaction within NiO compared with bulk NiO with large size. When used for a lithium-ion battery, NiO@HCS possesses the high capacity and superior rate capability as an anode material. Owing to the strong interaction of HCS and NiO crystals, NiO@HCS exhibits excellent cycle stability at a high current density. Furthermore, NiO@HCS also shows good capacitive performance in a symmetric supercapacitor device.

1. Introduction

The need for sustainable and renewable energy supply has become one of the greatest concerns in the twenty-first century because of the growing environmental and ecological crisis. Various electrochemical storage devices such as lithium-ion batteries (LIBs), electrochemical capacitors (ECs), and fuel cells (FCs) are attracting ever-increasing attention due to their cost-effectiveness and environmentally friendly properties compared to combustion-based energy technologies. When LIBs were firstly introduced into the market in 1991, they have been regarded as one of the most promising and efficient energy storage systems because they exhibited long lifetime and high energy density [1,2]. Nevertheless, LIBs still cannot meet the fast increasing requirements of great power and energy density, excellent cycling stability, and superior reversible and rate capability in our daily life [3,4]. Materials which can be used to assemble the electrode hold the key to improve the properties of LIBs [5–7]. Since commercial graphite anode exhibits a theoretical capacity of 372 mAh g^{-1}, much progress has been made with the anode materials [8–11]. In the past decades, transition metal oxides with remarkable electrochemical activity have emerged as new choices for electrochemical energy storage devices [12–16]. Among them, nickel oxide (NiO) owning a big theoretical specific capacity (718 mA h g^{-1}) has been regarded as a promising candidate as electrode materials. Its properties such as low cost, natural abundance and environmental friendliness have broadened its application for next-generation LIBs [17–19]. However, it shows some intrinsic disadvantages like the volume expansion/extraction/aggregation during the electrochemical reaction process and low electronic conductivity, leading to serious capacity fade and poor cycling stability. To address this issue, a variety of strategies have been developed, such as structural engineering [20,21],

* Corresponding author. Nanomaterials Physicochemistry Department, Faculty of Chemical Technology and Engineering, West Pomeranian University of Technology, Szczecin, Piastów Ave. 42, 71-065, Szczecin, Poland.
** Corresponding author.
*** Corresponding author.
E-mail addresses: xchen@zut.edu.pl (X. Chen), ttang@ciac.ac.cn (T. Tang), emijowska@zut.edu.pl (E. Mijowska).

https://doi.org/10.1016/j.jallcom.2019.05.147
0925-8388/

hybridization with conductive matrices [22], as well as mixed transition-metal oxides [23,24].

To date, NiO has been synthesized into various structures such as nanosheets [25,26], nanowires [27], nanotubes [28], nanofibers [29,30], and hollow spheres [31,32] in LIBs. Especially, three-dimensional (3D) hollow structures which possess large specific area for electrolyte contact can help to improve the capacity of NiO anode, but still suffer from the volume changing and capacity loss due to the poor electrical conductivity and weak mechanical stability [33,34]. Hence, flexible and conductive carbon materials such as amorphous carbon, graphene and carbon nanotubes (CNTs) have been used in preparing composites (NiO-C), achieving promising progress [35–37]. Besides, researchers tried to combine the two strategies together by designing bowl-like NiO nanosheets@carbon [38], metal-organic frameworks (MOFs) derived NiO/Ni/Graphene composites with hierarchical hollow structure [39], growing NiO nanosheets on hollow carbon spheres (HC@NiO) [40], et al. Benefiting from the two strategies, composites with hollow structures can not only improve the electrical conductivity, but also maintain the structural stability and excellent electrochemical performance. However, in those strategies, NiO structures are usually grown on the outer surface of carbon materials. Recently, a confinement strategy has emerged to grow nanostructures in hollow carbon materials to improve their electrochemical properties. SnS_2 nanosheets confined growth in carbon materials, exhibited excellent performance for sodium-ion batteries [41]. Although the outer carbon shells have been proved to increase the conductivity and reduce large volume expansion, the carbon materials produced under a lower temperature to avoid reduction of metal oxide are of low graphitization [41,42]. It is of great interest to figure out a strategy to encapsulate nanostructured NiO into a completed hollow carbon sphere, especially directly attaching to the inner carbon shell.

Due to the internal space of HCS, it is a perfect container for low-conductivity materials [43–45]. Herein, we demonstrate a strategy to prepare the hybrid structure of NiO crystals confined growing on the interior shells of HCS (Fig. 1a). The as-prepared NiO@HCS offers advantages as follows: (1) high surface-to-volume ratio giving rich electroactive sites, (2) suitable mesopores providing short diffusion paths for electrolyte, (3) enhanced electrical conductivity caused by the direct contact between NiO and interior carbon shell, (4) small size of NiO crystals formed from the confined Ni^{2+} after being filtrated through pores of HCS, which can provide more efficient lithiation/delithiation within NiO compared with bulk NiO with large size, (6) superior mechanical properties stabled by the strong link of HCS. The electrochemical performance of NiO@HCS was evaluated by cyclic voltammograms (CV) and galvanostatic charge-discharge (GCD). NiO@HCS electrode possesses large capacity, good capability and superior rate cycle stability.

2. Experimental section

2.1. Synthesis of NiO@HCS

Hollow carbon spheres were synthesized using a hard sacrificial template (amine-modified silica spheres) and a carbon source (glucose) [46]. Basically, amine-modified silica spheres (0.6 g) were mixed with glucose (0.6 g) aqueous solution (50 mL) under stirring for 2 h and then transferred into an autoclave for hydrothermal treatment at 180 °C for 12 h. The brown precipitate named as SiO_2@glucose was washed by filtration and dried up for further calcination treatment at 800 °C for 3 h. After removal of silica template by hydrofluoric acid, the product (HCS, 50 mg) was dissolved in ethanol and then 1 mL $Ni(NO_3)_2 \cdot 6H_2O$ solution (10 M in ethanol) was mixed with the above solution under sonication and stirred for 4 h. After washed by filtration, the mixture was heated in a furnace at 300 °C for 1 h under N_2 flow to get the final product NiO@HCS.

2.2. Electric measurements

HCS or NiO@HCS was mixed with polyvinylidene difluoride (PVDF, Solvay) and commercial carbon black (the mass ratio: 8: 1: 1) in 1-Methyl-2-pyrrolidone (NMP, Sigma) to obtain carbon slurries. Then the slurries were pasting on Cu foils as working electrodes and dried at 70 °C for 12 h under vacuum. For LIBs, the 2032 coin-type cells were assembled using an above-mentioned working electrode and a lithium foil (Aldrich) as the counter electrode. A commercial electrolyte of 1 M $LiPF_6$ in ethylene carbonate (EC)/dimethyl carbonate (DMC) (1:1 by volume) (SelectiLyte™ LP30) was used to assemble the cells in an argon-filled glove box. The electrochemical performance was carried out in the voltage range

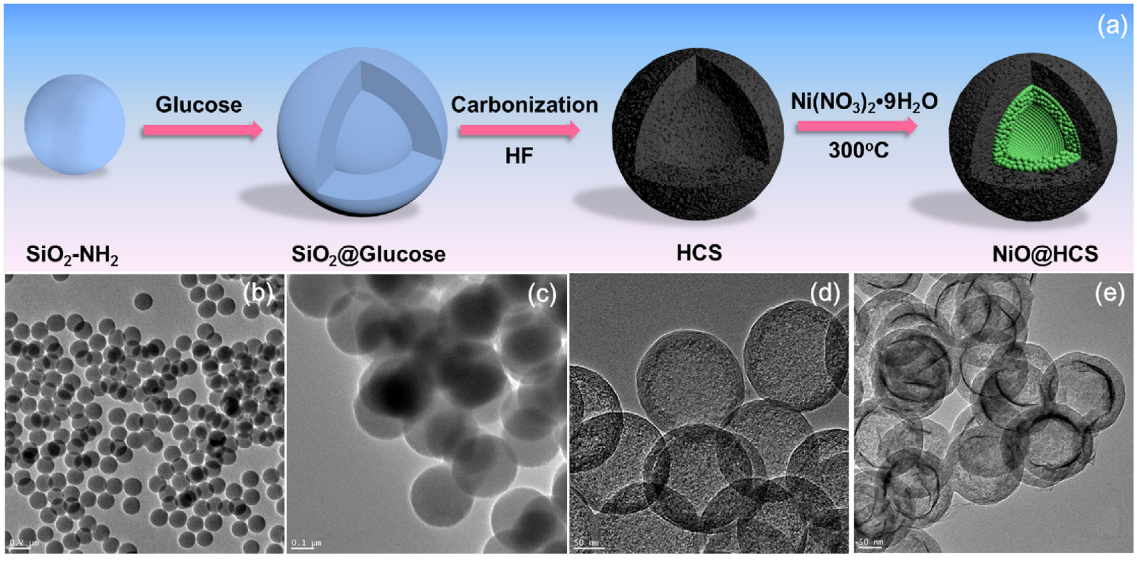

Fig. 1. (a) Schematic illustration of the preparation of NiO@HCS. TEM images of (b) amine-modified silica spheres (SiO_2-NH_2), (c) SiO_2@glucose spheres, (d) HCS, and (e) NiO@HCS.

of 0.01–3 V by using GCD and CV techniques with an EC-LAB VMP (BioLogic Science Instruments). For symmetric supercapacitor, two electrodes with each mass of 2 mg were prepared as the working electrode in LIBs. 6 M KOH aqueous solutions were used as the electrolyte. The electrochemical performance was evaluated by GCD and CV with a potential window from 0 to 1 V.

2.3. Characterization

Scanning electron microscopy (SEM, Hitachi SU8020), transmission electron microscopy (TEM, FEI) and X-ray diffraction (XRD, Philips) were carried out to measure the structural properties. The elemental mappings were performed on a scanning transmission electron microscope (STEM, FEI) to determine the elemental composition. The thermogravimetric analysis (TGA, DTA-Q600) under flowing air was performed to calculate the NiO content. The porosity was studied by N_2 adsorption/desorption isotherms (Micromeritics).

3. Results and discussion

The experimental details are illustrated in Fig. 1a. Choosing amine-functionalized silica spheres as the hard template is to make use of the abundant cationic ammonium groups (-NH_3^+), which can interact with the hydroxyl groups of glucose through electrostatic reaction. After glucose fully covered on the silica surface, it transformed to carbon under carbonization, forming a porous shell of HCS. When dissolving HCS into ethanol, the cavity of HCS can be filled with ethanol. And the porous shells allow nickel precursors diffusion into the cavity of HCS after adding nickel precursors to the HCS solution due to the concentration gradient between the interior ethanol and outer Ni^{2+}-containing ethanol. Ni^{2+} ions were adsorbed to the interior shells because of the negatively charged carbon. When washed by water, those physically adsorbed Ni^{2+} ions were easily removed while the inside nickel precursors still remained. Thus, after annealing at 300 °C, only NiO formed on the interior shells obtained.

The morphology of each material was investigated by TEM (Fig. 1). It can be observed that the silica spheres with a narrow diameter distribution of about 170 nm were dispersed homogenously (Fig. 1b). The samples obtained from the hydrothermal process shown in Fig. 1c have increased diameter from 170 to 210 nm, indicating silica spheres were covered by glucose separately. After carbonization and removing the silica core, the thickness of shells for HCS is about 20 nm, which can be verified by Fig. 1d. Besides, the strong contrast between the dark edge and apparent cavities indicate the hollow structures. In addition, the rough surface of HCS reveals a disorder porous texture of the shell. We surmise those pores resulted from the evaporation of H_2O and CO_2 during the carbonization process. Those porous shells could allow nickel precursors easy diffusion into the cavity of HCS. In Fig. 1e, a thin dark layer of NiO crystals can be observed in each cavity of HCS. There are crystals neither on the outer surface nor inside the shell for this final product under high-resolution TEM (Fig. S1), which further confirmed the NiO only formed in the interior carbon shells. The amounts of NiO crystal were controlled because after very few nickel precursors attached to the interior carbon shells, the diffusion was controlled because of sealed pores.

To further characterize the resulting NiO@HCS samples, SEM was used. Fig. 2a and b show the morphology of HCS and NiO@HCS, from which the hollow structures can be revealed by the broken spheres. Both HCS and NiO@HCS obtain a monodispersed sphere size. After confined loading with NiO, the spherical structure is still maintained. To be noted, there are no obvious dissociative nanoparticles and nanoparticle aggregations on the surface of HCS in Fig. 2b, which suggests the presence of NiO can only be inside the HCS. Energy-dispersive X-ray spectroscopy (EDS) mapping analysis has shown that almost all Ni and O are surrounding the shell of HCS. The Ni distribution together with the TEM image (Fig. 1e) can imply the confined presence of NiO with the inner shell of HCS. The close connection between NiO and HCS are believed to have a good effect on the electric conductivity and stability of NiO@HCS.

Fig. 3a shows the characterization of HCS and NiO@HCS by XRD. Two wide peaks at 2θ of 23.4° and 43.8° in HCS pattern are assigned to typical carbon (002) and (100) diffractions. An obvious carbon (002) diffraction peak still maintained observed from NiO@HCS pattern and a series of diffraction peaks at 2θ of 36.5°, 43.1°, and 62.0° correspond to the (111), (200), and (220) planes of NiO (JCPDS 47-1049), revealing an overlay of HCS and pure NiO. The weight percentage of NiO in the composite is determined by TGA, conducted with a heating rate of 10 °C/min in the air (Fig. 3b). Negligible weight was remained in HCS after raising temperature to 900 °C, revealing the composition of pure carbon. The mass ratio of NiO is determined to be 12.7 wt%. The porosity structures of HCS and NiO@HCS were characterized by N_2 adsorption-desorption experiment. The type IV isotherms with distinct hysteresis loops shown in Fig. 3c suggest the mesoporous structure. The specific surface area of HCS is 719 $m^2 g^{-1}$ calculated by Brunauer-Emmett-Teller (BET) method, while the value for NiO@HCS is still maintained with 418 $m^2 g^{-1}$. Pore size distribution is shown in Fig. 3d, which clearly confirms the presence of micropores and small mesopores, and the average pore size decreased from 4.2 to 3.8 nm after encapsulated NiO in HCS (Table S1). Besides, the micropore and mesopore volumes were obtained from N_2 absorption isotherm with the Barrett–Joyner–Halenda (BJH) method at different P/P_0 range (Table S1). The small decreases in micropore and mesopore volumes indicate the fair retention of micropores and mesopore in NiO@HCS, and suggest that the pores in carbon shells of HCS are not occupied by NiO crystals.

Fig. 4a and b are CV curves at a scan rate of 0.1 mV s^{-1} and GCD profiles a current density of 0.1 A g^{-1} for the beginning five cycles of HCS within the potential range of 0.01–3.0 V. The strong peak at 0.65 V which appears only in the first cycle is associated with a solid electrolyte interface (SEI) layer. After the first cycle, the scanning curves remain unchanged, suggesting high reversibility of HCS electrode. A small plateau at about 0.7 V can be observed from the first GCD profile, which is in accordance with the CV results. HCS anode delivers an initial discharge capacity of 752 mA h g^{-1} with an initial charge capacity of 381 mA h g^{-1} in the first cycle, revealing an initial Coulombic efficiency (CE) of 50.6% due to the SEI layer. The discharge and charge capacities of the 2nd cycle are 340 and 352 mA h g^{-1}, with an initial CE over 100%. And the CE values of the following cycles keep around 100%. To further investigate the rate behavior of HCS electrode, GCD profiles obtained by different applied current densities were presented (Fig. 4c). A sequential decay in reversible capacities as the rate increase can be observed. Fig. 4d shows that the electrode delivered reversible capacities of 343 mA h g^{-1}, 298 mA h g^{-1}, 271 mA h g^{-1}, 217 mA h g^{-1} and 187 mA h g^{-1} at current densities from 0.1 to 5 A g^{-1}. When decreasing the current density to 0.1 A g^{-1} again, the capacity quickly returned to 324 mA h g^{-1}. These results indicate an excellent rate capability.

To illustrate the electrochemical performance of NiO@HCS, we prepared an anode for LIBs based on this material. Fig. 5a shows the CV curves for the first five cycles at 0.1 mV s^{-1} within the potential range of 0.01–3.0 V vs. Li/Li+. There is a strong cathodic current peak at approximately 0.5 V in the first cycle, which is attributed to the reduction of NiO to Ni and the formation of amorphous Li_2O and SEI layer due to the electrolyte decomposition. To prove the formation of SEI, the LIB cell was disassembled after the first cycle. As

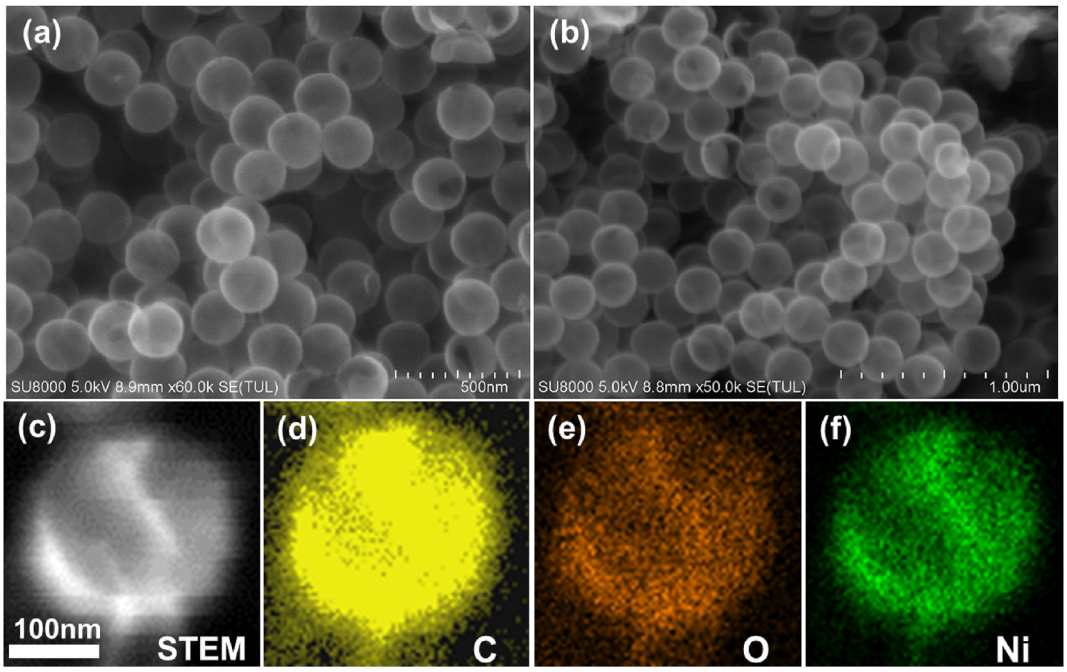

Fig. 2. SEM images of HCS (a) and NiO@HCS (b). (c) STEM image of a single NiO@HCS. (d–f) High-angle annular dark-field scanning transmission electron microscopy and energy-dispersive X-ray spectroscopy (HAADF-STEM-EDS) mapping images of NiO@HCS showing the carbon edge (d, yellow), oxygen edge (e, orange), and nickel edge (f, green). (For interpretation of the references to colour in this figure legend, the reader is referred to the Web version of this article.)

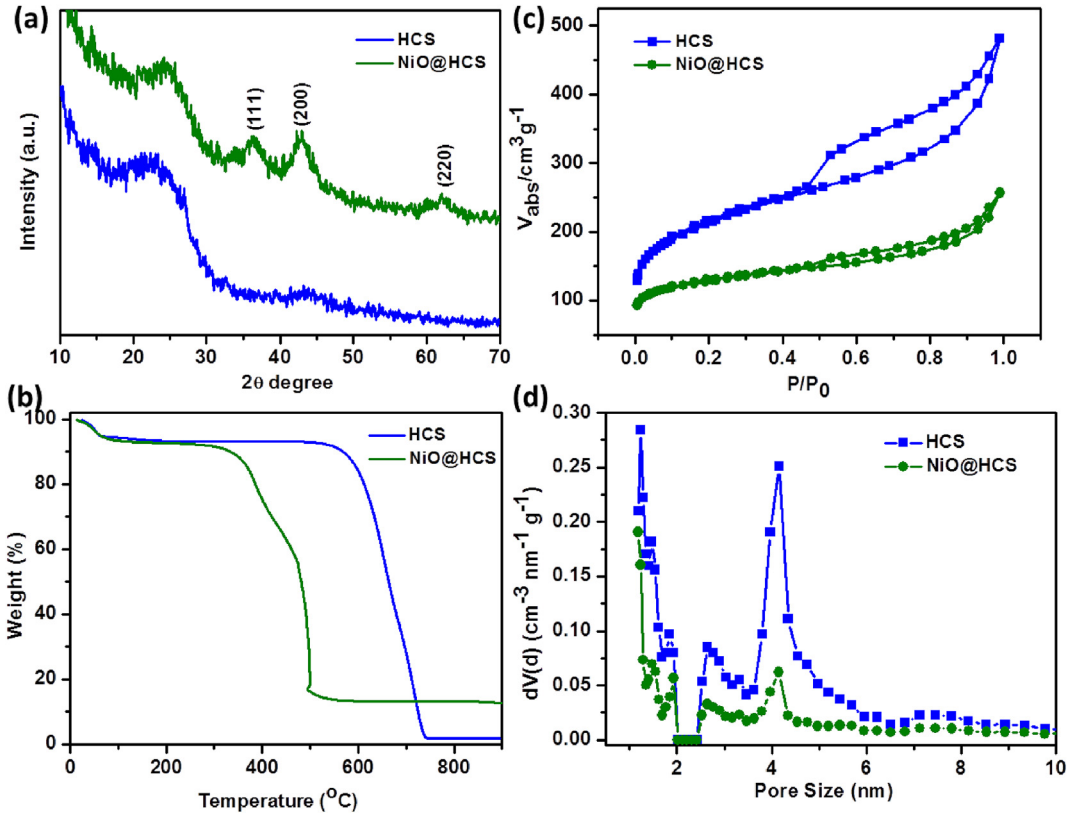

Fig. 3. (a) XRD, (b) TGA, (c) N_2 adsorption/desorption isotherms, and (d) pore size distributions of HCS and NiO@HCS.

revealed by Fig. S2, the SEI layer has already formed on the surface of NiO@HCS. However, a positive shift to about 0.9 V occurred with this cathodic current peak and the peak intensity decreased obviously during the following cycles, which may owe to the formation of the SEI layer and ultrafine NiO nanocrystals in the first scan [47–49]. In the first anodic curve, the two peaks at about 1.3 V

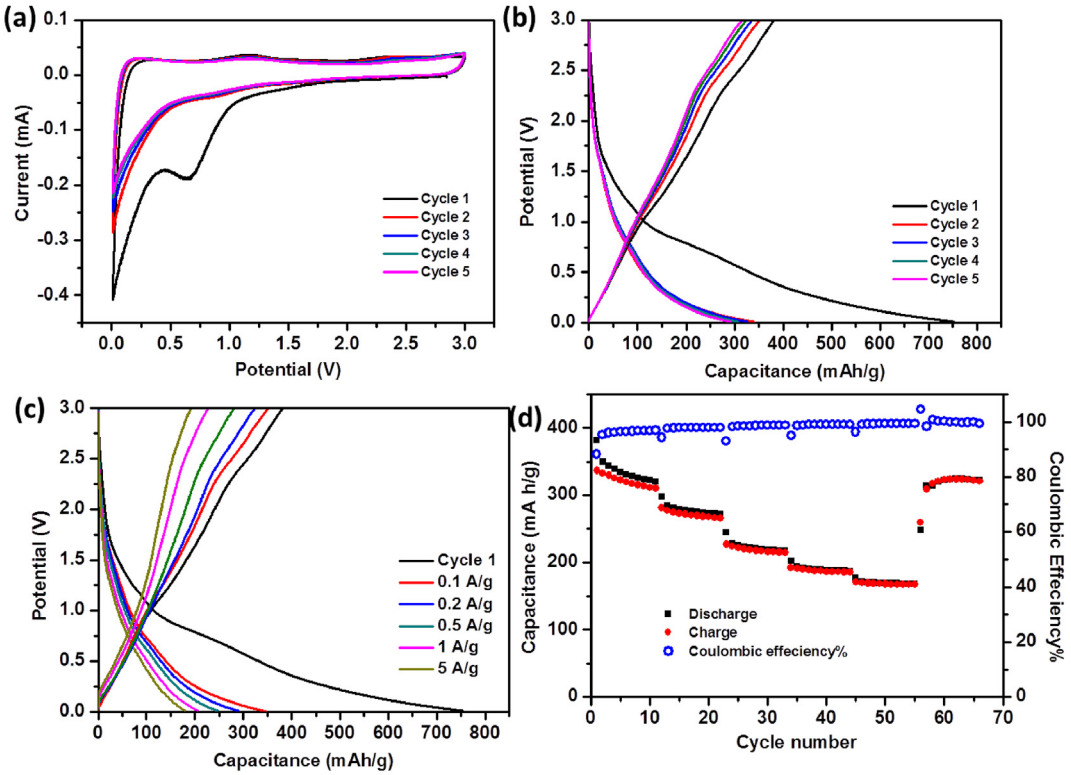

Fig. 4. Electrochemical performance of HCS: (a) cyclic voltammograms at a scan rate of 0.1 mV s^{-1} and (b) galvanostatic charge-discharge profiles at a current density of 0.1 A g^{-1} in the voltage range of 0.01–3.0 V; (c) voltage-capacity curves and (d) rate capability at different rates from 0.1 to 5 A g^{-1}.

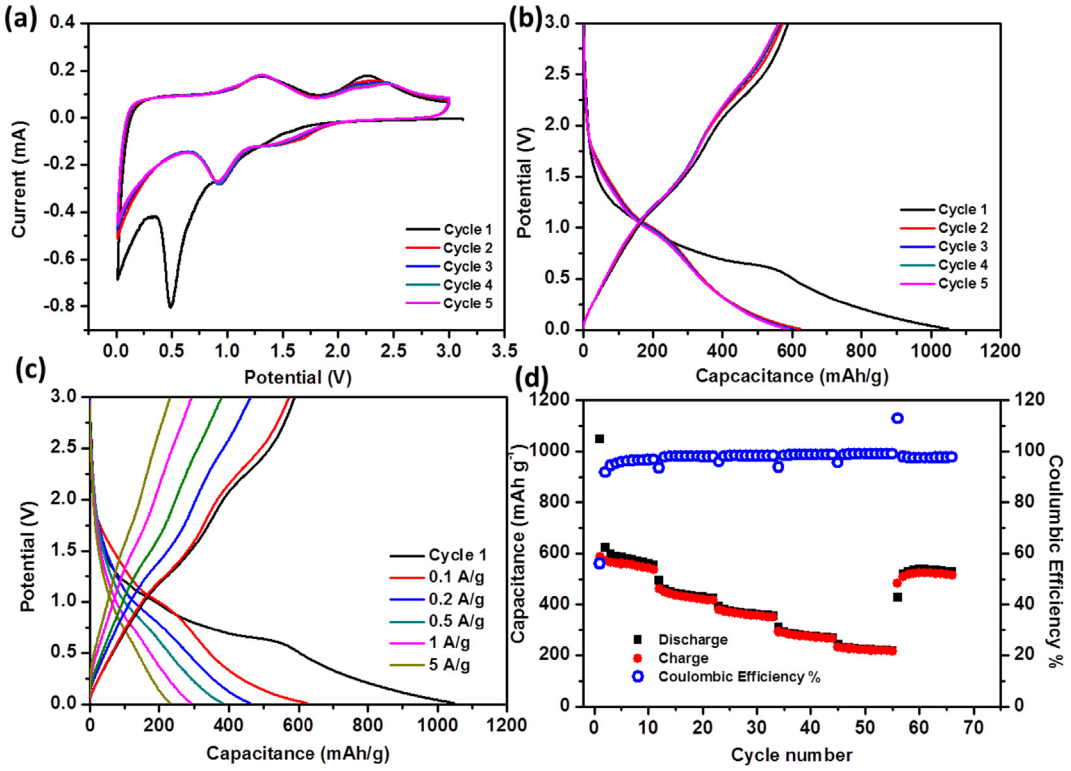

Fig. 5. Electrochemical performance of NiO@HCS: (a) CV at a scan rate of 0.1 mV s^{-1} and (b) GCD profiles at a current density of 0.1 A g^{-1} in the voltage range of 0.01–3.0 V; (c) voltage-capacity curves and (d) rate capability at different rates from 0.1 to 5 A g^{-1}.

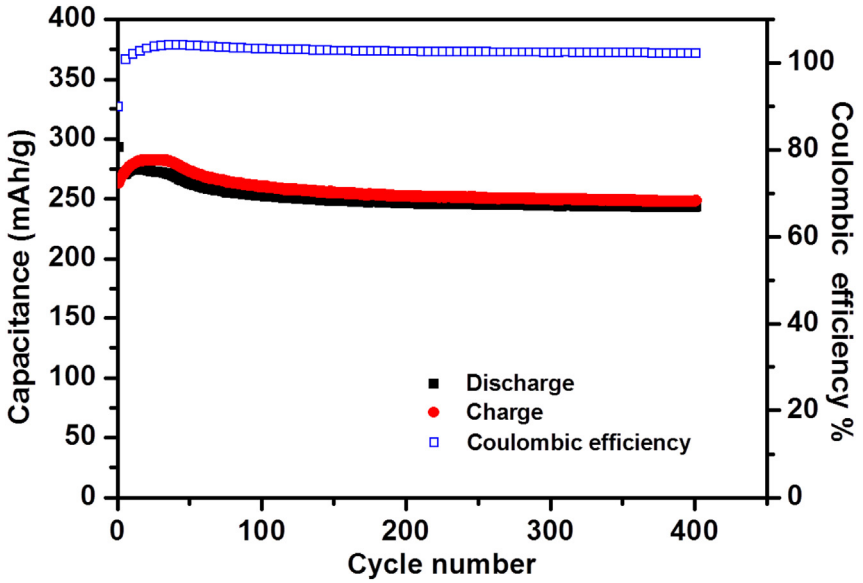

Fig. 6. Long cycling performance of NiO@HCS at a current density of 2 A g^{-1}.

and 2.3 V correspond to the partial decomposition of the SEI film and the conversion of Ni into NiO, respectively. What's more, the following CV profiles after the first cycle remain well overlapped, suggesting high reversibility of electrochemical reactions and good cycle stability of NiO@HCS. Fig. 5b shows the initial 5 GCD profiles of NiO@HCS at a constant current density of 0.1 A g^{-1}. The black lines represent the first cycle with initial discharge and charge capacities of 1048 and 588 mA h g^{-1}, respectively, for which the contributed capacities of HCS are calculated as 662 and 335 mA h g^{-1}, respectively. Based on the mass of NiO, the actual capacity value is calculated to be over 2000 mA h g^{-1} for the first cycle, which is much higher than the theoretical value of NiO (718 mA h g^{-1}). This could be ascribed to the SEI layers which can trap lithium in the active material and provide extra lithium storage capacity, as well as the synergetic effect between HCS and NiO providing more efficient utilization of the active material [50]. This phenomenon is common for NiO. The CE of the first cycle is as low as 56%, which could be due to the SEI layer and the trapping of part lithium in the active material. The subsequent discharge and charge process can deliver a discharge capacity of 624 mA h g^{-1}, with the corresponding charge capacity of 572 mA h g^{-1}. Capacities of NiO@HCS remain stable after the first cycle with much higher CE (>90%), indicating reversible redox reactions.

Rate capability is an important factor for LIBs. We further evaluate the rate capabilities of NiO@HCS electrode at different current densities ranging from 0.1 to 5 A g^{-1}. Fig. 5c shows GCD profiles of NiO@HCS at different current densities. A decrease from capacity values can be observed as the increasing applied current density. In detail, as shown in Fig. 5d, the electrode delivered reversible capacities of 598 mA h g^{-1}, 490 mA h g^{-1}, 395 mA h g^{-1}, 312 mA h g^{-1} and 231 mA h g^{-1} with the increasing current density. After resetting the current density back to 0.1 A g^{-1}, the capacity quickly returned to 484 mA h g^{-1}. When the current density reset to the initial value, the capacity recovered, demonstrating a good rate capability. It is obvious that NiO@HCS shows high capacity at a high current density and excellent rate capability due to the structural properties and the fine NiO crystals which allow fast electrolyte diffusion and electron transport, as well as efficient lithium insertion/extraction.

Cycling stability which is another key issue for evaluating the behavior of electrode materials was tested at 2 A g^{-1} for NiO@HCS anode. As can be seen in Fig. 6, NiO@HCS exhibits a discharge capacity of 243 mA h g^{-1} after 400 cycles with a high current density. The capacity retention to the first discharge capacity is about 83%. And the morphology of NiO@HCS after 400 cycles at 2.0 A g^{-1} was revealed by Fig. S3. The spherical morphology maintained well after long cycles suggested the high structural stability of NiO@HCS. The corresponding CE is close to 100%, indicating that NiO@HCS has good reversibility for Li^+ insertion/extraction. As shown in Table 1, NiO@HCS exhibits good capacity compared to the state of the art, and obtains enhanced cycling stability for 400 cycles at a high current rate.

Table 1
Summary of representative NiO/C anode materials for LIBs.

Electrode	Current (mA g^{-1})	Initial C_{dis}/C_{cha} (mAh g^{-1})	Cycle number	Capacity retention	Refs.
NiO-G-Ni	125	936/734	150	78%	[51]
CYS-NiO/C	1000	1124/778	500	88%	[52]
NiO/MWCNT	50	1084/720	50	74%	[53]
NiO-C	100	1155/715	50	35%	[54]
NiO/C	100	1175/-	100	53%	[55]
NiO@C	100	913/677	50	91%	[56]
C-coated Ni/NiO	100	1600/-	100	96%	[57]
NiO-NFAs@GNSs	100	957/608	100	41	[58]
NiO-NPs@GNSs		967/629		77	
G-Ni-G	71.8	1164/639	50	54	[59]
NiO@HCS	100	1048/588	400	83%	This work

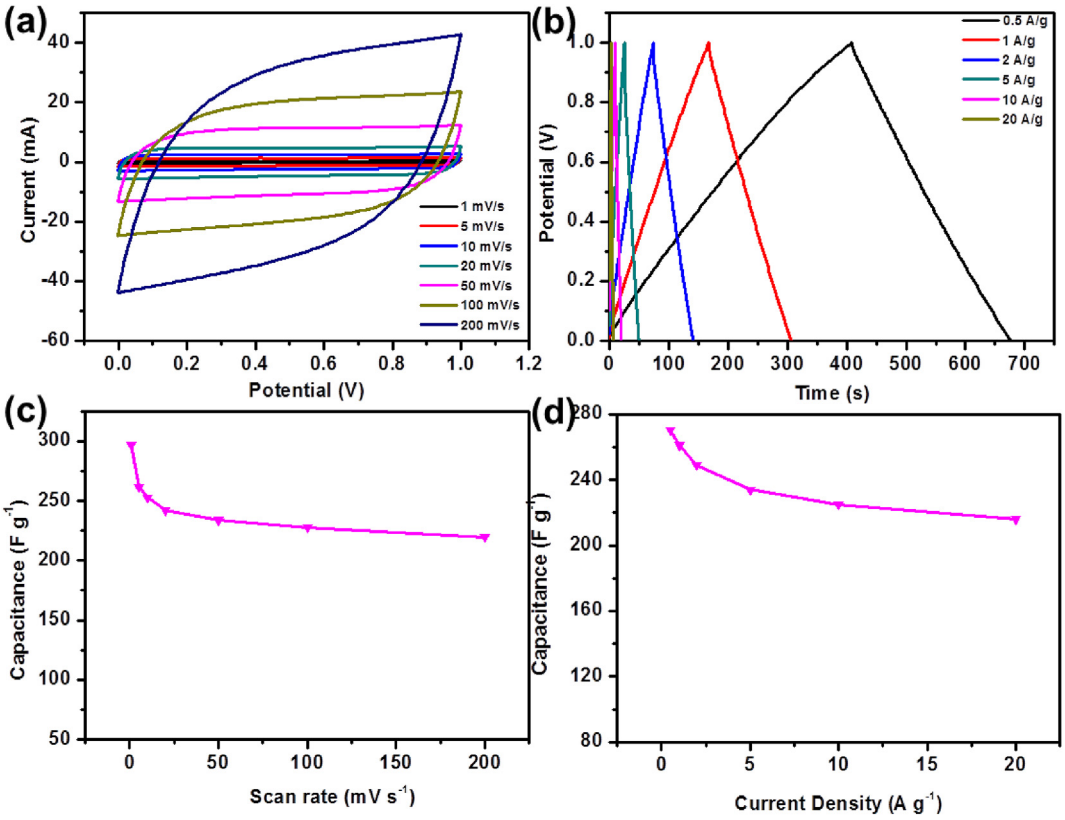

Fig. 7. Symmetric pseudocapacitor performances of NiO@HCS in 6 M KOH. (a) CV curves at applied scan rates from 1 to 200 mV s^{-1}. (b) GCD curves at applied current densities from 0.5 to 20 A g^{-1}. (c, d) Variations of specific capacitances.

Inspired by the excellent results from LIBs, the symmetric capacitor was constructed by the NiO@HCS. CV curves display a small deviation from a rectangle due to the Faradaic reaction but without obvious peaks for water decomposition (Fig. 7a). GCD curves with different current densities are all triangular in shape, suggesting good reversibility (Fig. 7b). And the good linearity of GCD curves indicates a stable behavior at high potential. NiO@HCS obtained a large specific capacitance of 297 F g^{-1} (Fig. 7c) owing to the Faradaic capacitance contributed by NiO, of which the value is 1012 F g^{-1} in consideration of the low content of NiO (12.7 wt%). This great contribution of NiO reveals efficient Faradaic reaction between electrolyte and electrode. The specific capacitances calculated from GCD curves are in accordance with CV results, and maintained 80% of the capacitance from 0.5 to 20 A g^{-1} (Fig. 7d), demonstrating its good rate performance. Besides, the cavity of NiO@HCS can store electrolyte for deeper diffusion, and ultrathin NiO crystals can provide more accessible active sites for electrolyte ions. This synergistic effect helps to improve the capacitance and rate stability of NiO@HCS.

4. Conclusions

In summary, a unique NiO@HCS hollow structure was selectively prepared, providing large electrode/electrolyte contact area and interior space for extra Li^+ storage. Porous carbon shells with a thin layer allow fast lithium ion diffusion and electron transportation. As the anode material for LIBs, NiO@HCS delivers a reversible capacity of 598 mA h g^{-1} at 0.1 A g^{-1} and exhibits a discharge capacity of 243 mA h g^{-1} after 400 cycles at a high current density of 2 A g^{-1}. For supercapacitor investigation, NiO@HCS also exhibits a high specific capacitance of 297 F g^{-1} based on a symmetric configuration. The electrochemical performance of NiO@HCS can be further optimized via tuning shell thickness and core size. Moreover, such structures are also fit for other transition metal oxides, sulfur, or silicon, providing further applications.

Acknowledgments

The authors acknowledge financial support from the National Science Centre, Poland, within UMO-2016/23/G/ST5/04200.

Appendix A. Supplementary data

Supplementary data to this article can be found online at https://doi.org/10.1016/j.jallcom.2019.05.147.

References

[1] B. Dunn, H. Kamath, J.M. Tarascon, Electrical energy storage for the grid: a battery of choices, Science 334 (2011) 928–935.
[2] V. Etacheri, R. Marom, R. Elazari, G. Salitra, D. Aurbach, Challenges in the development of advanced Li-ion batteries: a review, Energy Environ. Sci. 4 (2011) 3243–3262.
[3] J.M. Tarascon, M. Armand, Issues and challenges facing rechargeable lithium batteries, Nature 414 (2001) 359–367.
[4] J.B. Goodenough, Y. Kim, Challenges for rechargeable Li batteries, Chem. Mater. 22 (2010) 587–603.
[5] A.S. Arico, P. Bruce, B. Scrosati, J.M. Tarascon, W. Van Schalkwijk, Nanostructured materials for advanced energy conversion and storage devices, Nat. Mater. 4 (2005) 366–377.
[6] B. Kang, G. Ceder, Battery materials for ultrafast charging and discharging, Nature 458 (2009) 190–193.
[7] C. Liu, F. Li, L.P. Ma, H.M. Cheng, Advanced materials for energy storage, Adv. Mater. 22 (2010) E28–E62.
[8] X. Chen, Y. Huang, K. Zhang, Cobalt nanofibers coated with layered nickel silicate coaxial core-shell composites as excellent anode materials for lithium ion batteries, J. Colloid Interface Sci. 513 (2018) 788–796.

[9] X. Chen, Y. Huang, K. Zhang, X. Feng, M. Wang, Synthesis and high-performance of carbonaceous polypyrrole nanotubes coated with SnS_2 nanosheets anode materials for lithium ion batteries, Chem. Eng. J. 330 (2017) 470–479.

[10] X. Chen, Y. Huang, K. Zhang, X. Feng, M. Wang, Porous TiO_2 nanobelts coated with mixed transition-metal oxides Sn_3O_4 nanosheets core-shell composites as high-performance anode materials of lithium ion batteries, Electrochim. Acta 259 (2018) 131–142.

[11] X. Chen, Y. Huang, X. Han, K. Zhang, Synthesis of cobalt nanofibers @ nickel sulfide nanosheets hierarchical core-shell composites for anode materials of lithium ion batteries, Electrochim. Acta 284 (2018) 418–426.

[12] P. Poizot, S. Laruelle, S. Grugeon, L. Dupont, J.M. Tarascon, Nano-sized transition-metaloxides as negative-electrode materials for lithium-ion batteries, Nature 407 (2000) 496–499.

[13] H.B. Wu, J.S. Chen, H.H. Hng, X.W. Lou, Nanostructured metal oxide-based materials as advanced anodes for lithium-ion batteries, Nanoscale 4 (2012) 2526–2542.

[14] W.M. Zhang, X.L. Wu, J.S. Hu, Y.G. Guo, L.J. Wan, Carbon coated Fe_3O_4 nanospindles as a superior anode material for lithium-ion batteries, Adv. Funct. Mater. 18 (2008) 3941–3946.

[15] X. Wang, X.L. Wu, Y.G. Guo, Y.T. Zhong, X.Q. Cao, Y. Ma, J.N. Yao, Synthesis and lithium storage properties of Co_3O_4 nanosheet-assembled multishelled hollow spheres, Adv. Funct. Mater. 20 (2010) 1680–1686.

[16] K.F. Zhong, X. Xia, B. Zhang, H. Li, Z.X. Wang, L.Q. Chen, MnO powder as anode active materials for lithium ion batteries, J. Power Sources 195 (2010) 3300–3308.

[17] H. Liu, G.X. Wang, J. Liu, S.Z. Qiao, H.J. Ahn, Highly ordered mesoporous NiO anode material for lithium ion batteries with an excellent electrochemical performance, J. Mater. Chem. 21 (2011) 3046–3052.

[18] B. Varghese, M.V. Reddy, Z. Yanwu, C.S. Lit, T.C. Hoong, G.V.S. Rao, B.V.R. Chowdari, A.T.S. Wee, C.T. Lim, C.H. Sow, Fabrication of NiO nanowall electrodes for high performance lithium ion battery, Chem. Mater. 20 (2008) 3360–3367.

[19] X.H. Wang, X.W. Li, X.L. Sun, F. Li, Q.M. Liu, Q. Wang, D.Y. He, Nanostructured NiO electrode for high rate Li-ion batteries, J. Mater. Chem. 21 (2011) 3571–3573.

[20] L. Liu, Y. Li, S.M. Yuan, M. Ge, M.M. Ren, C.S. Sun, Z. Zhou, Nanosheet-based NiO microspheres: controlled solvothermal synthesis and lithium storage performances, J. Phys. Chem. C 114 (2010) 251–255.

[21] X.H. Wang, Z.B. Yang, X.L. Sun, X.W. Li, D.S. Wang, P. Wang, D.Y. He, NiO nanocone array electrode with high capacity and rate capability for Li-ion batteries, J. Mater. Chem. 21 (2011) 9988–9990.

[22] Y.Q. Zou, Y. Wang, NiO nanosheets grown on graphene nanosheets as superior anode materials for Li-ion batteries, Nanoscale 3 (2011) 2615–2620.

[23] C.Z. Yuan, H.B. Wu, Y. Xie, X.W. Lou, Mixed transition-metal oxides: design, synthesis, and energy-related applications, Angew. Chem. Int. Ed. 53 (2014) 1488–1504.

[24] Y. Sharma, N. Sharma, G.V.S. Rao, B.V.R. Chowdari, Nanophase $ZnCo_2O_4$ as a high performance anode material for Li-ion batteries, Adv. Funct. Mater. 17 (2007) 2855–2861.

[25] X.H. Wang, L. Qiao, X.L. Sun, X.W. Li, D.K. Hu, Q. Zhang, D.Y. He, Mesoporous NiO nanosheet networks as high performance anodes for Li ion batteries, J. Mater. Chem. A 1 (2013) 4173–4176.

[26] P. Subalakshmi, A. Sivashanmugam, Fuel aided synthesis of NiO flakes for electrochemical energy storage application, J. Alloys Compd. 662 (2016) 200–207.

[27] V. Aravindan, P.S. Kumar, J. Sundaramurthy, W.C. Ling, S. Ramakrishna, S. Madhavi, Electrospun NiO nanofibers as high performance anode material for Li-ion batteries, J. Power Sources 227 (2013) 284–290.

[28] S.A. Needham, G.X. Wang, H.K. Liu, Synthesis of NiO nanotubes for use as negative electrodes in lithium ion batteries, J. Power Sources 159 (2006) 254–257.

[29] S. Hwan Oh, J.-S. Park, M. Su Jo, Y.C. Kang, J.S. Cho, Design and synthesis of tube-in-tube structured NiO nanobelts with superior electrochemical properties for lithium-ion storage, Chem. Eng. J. 347 (2018) 889–899.

[30] J.S. Cho, S.Y. Lee, H.S. Ju, Y.C. Kang, Synthesis of NiO nanofibers composed of hollow nanospheres with controlled sizes by the nanoscale kirkendall diffusion process and their electrochemical properties, ACS Appl. Mater. Interfaces 7 (2015) 25641–25647.

[31] X.H. Huang, J.P. Tu, C.Q. Zhang, F. Zhou, Hollow microspheres of NiO as anode materials for lithium-ion batteries, Electrochim. Acta 55 (2010) 8981–8985.

[32] J.S. Cho, J.M. Won, J.-H. Lee, Y.C. Kang, Synthesis and electrochemical properties of spherical and hollow-structured NiO aggregates created by combining the Kirkendall effect and Ostwald ripening, Nanoscale 7 (2015) 19620–19626.

[33] H.J. Wu, Y.Q. Wang, C.H. Zheng, J.M. Zhu, G.L. Wu, X.H. Li, Multi-shelled NiO hollow spheres: easy hydrothermal synthesis and lithium storage performances, J. Alloys Compd. 685 (2016) 8–14.

[34] Y.Y. Yang, Y.R. Liang, Z.Y. Zhang, Y.D. Zhang, H.Y. Wu, Z.A. Hu, Morphology well-controlled synthesis of NiO by solvothermal reaction time and their morphology-dependent pseudocapacitive performances, J. Alloys Compd. 658 (2016) 621–628.

[35] Y. Huang, X.L. Huang, J.S. Lian, D. Xu, L.M. Wang, X.B. Zhang, Self-assembly of ultrathin porous NiO nanosheets/graphene hierarchical structure for high-capacity and high-rate lithium storage, J. Mater. Chem. 22 (2012) 2844–2847.

[36] Y. Xia, W.K. Zhang, Z. Xiao, H. Huang, H.J. Zeng, X.R. Chen, F. Chen, Y.P. Gan, X.Y. Tao, Biotemplated fabrication of hierarchically porous NiO/C composite from lotus pollen grains for lithium-ion batteries, J. Mater. Chem. 22 (2012) 9209–9215.

[37] Y.J. Mai, S.J. Shi, D. Zhang, Y. Lu, C.D. Gu, J.P. Tu, NiO-graphene hybrid as an anode material for lithium ion batteries, J. Power Sources 204 (2012) 155–161.

[38] J. Liang, H. Hu, H. Park, C.H. Xiao, S.J. Ding, U. Paik, X.W. Lou, Construction of hybrid bowl-like structures by anchoring NiO nanosheets on flat carbon hollow particles with enhanced lithium storage properties, Energy Environ. Sci. 8 (2015) 1707–1711.

[39] F. Zou, Y.-M. Chen, K. Liu, Z. Yu, W. Liang, S.M. Bhaway, M. Gao, Y. Zhu, Metal organic frameworks derived hierarchical hollow NiO/Ni/graphene composites for lithium and sodium storage, ACS Nano 10 (2016) 377–386.

[40] B. Wang, G. Wang, X. Cheng, H. Wang, Synthesis and electrochemical investigation of core-shell ultrathin NiO nanosheets grown on hollow carbon microspheres composite for high performance lithium and sodium ion batteries, Chem. Eng. J. 306 (2016) 1193–1202.

[41] Y.H. Liu, X.Y. Yu, Y.J. Fang, X.S. Zhu, J.C. Bao, X.S. Zhou, X.W. Lou, Confining SnS_2 ultrathin nanosheets in hollow carbon nanostructures for efficient capacitive sodium storage, Joule 2 (2018) 725–735.

[42] Z.M. Liu, T.C. Lu, T. Song, X.Y. Yu, X.W. Lou, U. Paik, Structure-designed synthesis of FeS_2@C yolk-shell nanoboxes as a high-performance anode for sodium-ion batteries, Energy Environ. Sci. 10 (2017) 1576–1580.

[43] W.M. Zhang, J.S. Hu, Y.G. Guo, S.F. Zheng, L.S. Zhong, W.G. Song, L.J. Wan, Tin-nanoparticles encapsulated in elastic hollow carbon spheres for high-performance anode material in lithium-ion batteries, Adv. Mater. 20 (2008) 1160–1165.

[44] H.Y. Zhang, L.Q. Li, Z.P. Li, W.H. Zhong, H.Y. Liao, Z.H. Li, Controllable synthesis of SnO_2@carbon hollow sphere based on bi-functional metallo-organic molecule for high-performance anode in Li-ion batteries, Appl. Surf. Sci. 442 (2018) 65–70.

[45] X.L. Liu, Y.X. Chen, H.B. Liu, Z.Q. Liu, SiO_2@C hollow sphere anodes for lithium-ion batteries, J. Mater. Sci. Technol. 33 (2017) 239–245.

[46] Y. Han, X. Dong, C. Zhang, S. Liu, Hierarchical porous carbon hollow-spheres as a high performance electrical double-layer capacitor material, J. Power Sources 211 (2012) 92–96.

[47] S.H. Oh, M.S. Jo, S.M. Jeong, Y.C. Kang, J.S. Cho, Hierarchical yolk-shell CNT-(NiCo)O/C microspheres prepared by one-pot spray pyrolysis as anodes in lithium-ion batteries, Chem. Eng. J. 368 (2019) 438–447.

[48] J.S. Cho, J.-S. Park, K.M. Jeon, Y. Chan Kang, 1-D nanostructure comprising porous Fe_2O_3/Se composite nanorods with numerous nanovoids, and their electrochemical properties for use in lithium-ion batteries, J. Mater. Chem. A 5 (2017) 10632–10639.

[49] J.H. Lee, S.H. Oh, S.Y. Jeong, Y.C. Kang, J.S. Cho, Rattle-type porous Sn/C composite fibers with uniformly distributed nanovoids containing metallic Sn nanoparticles for high-performance anode materials in lithium-ion batteries, Nanoscale 10 (2018) 21483–21491.

[50] J. Wu, W.-J. Yin, W.-W. Liu, P. Guo, G. Liu, X. Liu, D. Geng, W.-M. Lau, H. Liu, L.-M. Liu, High performance NiO nanosheets anchored on three-dimensional nitrogen-doped carbon nanotubes as a binder-free anode for lithium ion batteries, J. Mater. Chem. A 4 (2016) 10940–10947.

[51] X. Chen, T. Xiao, S. Wang, J. Li, P. Xiang, L. Jiang, X. Tan, Superior Li-ion storage performance of graphene decorated NiO nanowalls on Ni as anode for lithium ion batteries, Mater. Chem. Phys. 222 (2019) 31–36.

[52] M.S. Jo, S. Ghosh, S.M. Jeong, Y.C. Kang, J.S. Cho, Coral-like yolk–shell-structured nickel oxide/carbon composite microspheres for high-performance Li-ion storage anodes, Nano-Micro Lett. 11 (2019) 3.

[53] C. Xu, J. Sun, L. Gao, Large scale synthesis of nickel oxide/multiwalled carbon nanotube composites by direct thermal decomposition and their lithium storage properties, J. Power Sources 196 (2011) 5138–5142.

[54] M.M. Rahman, S.-L. Chou, C. Zhong, J.-Z. Wang, D. Wexler, H.-K. Liu, Spray pyrolyzed NiO–C nanocomposite as an anode material for the lithium-ion battery with enhanced capacity retention, Solid State Ionics 180 (2010) 1646–1651.

[55] G. Li, Y. Li, J. Chen, P. Zhao, D. Li, Y. Dong, L. Zhang, Synthesis and research of egg shell-yolk NiO/C porous composites as lithium-ion battery anode material, electrochim, Acta 245 (2017) 941–948.

[56] G. Zhou, J. Ma, L. Chen, Selective carbon coating techniques for improving electrochemical properties of NiO nanosheets, Electrochim. Acta 133 (2014) 93–99.

[57] Y. Luo, M. Weng, J. Zheng, Q. Zhang, B. Xu, S. Song, Y. Shen, Y. Lin, F. Pan, C. Nan, The origin of cycling enhanced capacity of Ni/NiO species confined on nitrogen doped carbon nanotubes for lithium-ion battery anodes, J. Alloys Compd. 750 (2018) 17–22.

[58] L. Zhuo, Y. Wu, W. Zhou, L. Wang, Y. Yu, X. Zhang, F. Zhao, Trace amounts of water-induced distinct growth behaviors of NiO nanostructures on graphene in CO_2-expanded ethanol and their applications in lithium-ion batteries, ACS Appl. Mater. Interfaces 5 (2013) 7065–7071.

[59] W. Yue, S. Jiang, W. Huang, Z. Gao, J. Li, Y. Ren, X. Zhao, X. Yang, Sandwich-structural graphene-based metal oxides as anode materials for lithium-ion batteries, J. Mater. Chem. A 1 (2013) 6928–6933.